sciendo

DOI 10.2478/ama-2024-0038

acta mechanica et automatica, vol.18 no.2 (2024)

NUMERICAL MODELLING AND SIMULATION OF THE SHEAR-SLITTING PROCESS OF ELECTRICAL STEELS

Łukasz BOHDAL*, Agnieszka KUŁAKOWSKA*, Marcin KUŁAKOWSKI*

*Faculty of Mechanical Engineering, Koszalin University of Technology, ul. Racławicka 15-17, 75-620 Koszalin, Poland

lukasz.bohdal@tu.koszalin.pl, agnieszka.kulakowska@tu.koszalin.pl, marcinkulakowski@wp.pl

received 19 June 2023, revised 10 November 2023, accepted 3 December 2023

Abstract: Despite the development of laser processing, the mechanical cutting process is still widely used in the formation of electric steels that are very sensitive to thermal phenomena. However, proper process control is difficult due to the large number of factors determining the quality of the products. As a result, the quality of the cut edge is characterised by the presence of burrs, the removal of which increases the production costs. Due to their magnetic properties, these materials should not be exposed to excessive stresses and deformations. The article presents the possibilities of predicting the characteristic features of the cut edge as well as stress distributions in this area. Original shear-slitting finite element method (FEM) models were developed, the results of which were verified experimentally. The proposed method based on stress triaxiality analysis enables precise analysis of stress states in the cutting zone and the boundaries of the slip fracture transition in the separating fracture, as well as determining the method of material cracking. Variable control factors such as cutting clearance, rake angle of the upper knife, and cutting speed were taken into account in the models. Parametric analysis of the process was carried out and it was determined how the process parameters should be selected in order to obtain the appropriate quality of the product. The developed analysis results can be useful on production lines for proper process control.

Key words: shear-slitting, electrical steels, residual stress, triaxiality, sheared-edge

1. INTRODUCTION

In the process of cutting metal materials, it is very important to properly control the process in order to obtain the optimal technological quality of the product. It depends on both the characteristics of the cut surface and the dimensional and shape accuracy of the formed elements. In the processes of cutting thin materials such as electrical steel sheets or amorphous tapes in industrial conditions, there is a problem with the formation of burrs on the cut edge. Burrs are hard, sharp and raised edges created on the cut surface of the material during the process. They often have an irregular height along the cut line. The presence of burrs must be removed by further processing, such as machining or deburring, further increasing the cost of production [1]. The intensity of the increase in the height of the burrs increases with the wear of the cutting tool blades [2]. In the case of cutting thin sheets, it is also important to select the appropriate cutting clearance, so that the width of the deformed zone along the cut edge is as small as possible [3]. As research by the authors of papers [4–7] has shown, the clearance value should be selected depending on the cutting speed. Since the cutting process generates plastic strains and residual stresses that concentrate near the cutting edge of the sheet, it is necessary to have knowledge about the distribution of plastic strains and stresses in the cutting zone. According to many authors, the reason for the deterioration of the magnetic properties is the change in the flux density distribution due to material stresses and deformations [8–10]. In the works [8, 11], it was shown that the residual stresses after punching and blanking go further into the material than the strain-hardened area. According to studies, the zone of plastic deformation after mechanical cutting is at least 0.1 mm and grows rapidly with the increase in the wear of cutting tools [8, 12, 13]. Deformations along the cutting line may be the reason for the formation of an elastic stress zone in the depth of the material, adjacent to the plastically deformed area. As a result, both zones strongly influence the magnetic properties. In the case of aluminium sheets, the burr adversely affects the processes of joining sheets, while in the case of electrical steel sheets, on the packing in the magnetic cores. In the literature, there are known techniques for measuring the hardness of the sheet in the vicinity of the cut edge, aimed at determining the plastic state and the width of the deformation zone into the material. These are invasive methods that cause local changes in the magnetic properties in the measurement zone. The degree of degradation of magnetic properties also depends on factors such as chemical composition, type of material, type of cutting technique, technological parameters of the process, etc. Moreover, in the case of thin sheets, the measurement is subject to error [14–16].

In the available literature, many works focus on the analysis of the negative impact of punching and blanking processes on the magnetic properties of grain-oriented and non-grain oriented silicon electrical steel sheets [17, 18]. The impact of the blanking process, depending on the thickness of the non-grain oriented electrical steel and the deterioration of core losses was studied in Toda et al. [19] and Omura et al. [20]. It was found that the distribution of the hardness increase near the shear edge was almost half of the plate thickness for all the tested steels. The use of thinner steel sheets for the magnetic core could reduce the iron losses in the punching process. In works [21] and [22] it was

shown that electrotechnical steels with a high content of silicon and characterised by large grains are more sensitive to the deterioration of magnetic properties in the punching process. Subramonian et al. [23] determined the effect of the punching process parameters on various 0.25 mm and 0.8 mm thick steel sheets by means of experimental studies. The authors showed that blanking clearance is the most important factor influencing the quality of the cut edge. Its values must be selected depending on the thickness of the cut sheet and the type of material. An increase in clearance above a critical value causes a significant increase in burr on the cut surface. In work [24], the effect of grain size and banking clearance on selected magnetic characteristics was experimentally analysed. As a result of process optimisation, guidelines were proposed to reduce core losses by 5.8%. In the work [8], the impact of material grain size on iron losses after the blanking process and on the course of the blanking forces was assessed. In Wang et al. [14], the impact of the blanking process on the magnetic properties of non-oriented electrical steel sheets was analysed, focussing on the assessment of the degree of changes in magnetic properties depending on the increase in stress in the cutting zone. Variable geometry tools were used. With the help of appropriate tool geometries and clearance values, it was possible to limit the negative changes in magnetic properties.

Recent literature provides information on the characteristics of the width of the cut edge and new methods used to quantify its length. Problems with obtaining high-quality cut edges are indicated because deformations of the material domain walls occur and, as a consequence, the domain magnetisation flux decreases and the shift between the magnetisation flux and the total flux increases. Monitoring techniques are used to determine the characteristic features of the cut edge [25–28]. In paper [29], the relations between the relevant material parameters, i.e., sheet thickness, alloying and grain size and non-linear magnetic properties, are studied, with a focus on cut surface features and iron losses. Paper [30] presents an approach for image-based blanking tool wear monitoring and workpiece shape. The workpiece images offer the possibility to apply computer vision algorithms for handcrafted feature extraction in order to capture the cut surface formation and product properties as time-efficiently as possible. The work [31] analysed the causes of burr formation on the cut edge of blanked details. The authors indicated that the main cause of this is the wear of the cutting edges of the punch and die. The correct determination of the width of individual zones on the cut surface, and thus the prediction of the occurrence of areas with variable fracture mechanisms, is currently one of the main difficulties encountered in the literature related to mechanical cutting processes. According to the works [4, 9, 32, 33], the local state of stress in the shear zone is important for the formation of shear bands and significantly affects the topography of the cut surface. Higher local compressive stresses inhibit cracking and allow the material to flow plastically for longer periods.

The finite element method (FEM) is increasingly used in many industries as a powerful numerical tool to analyse physical phenomena occurring in various processes and to shorten the cycle time of introducing new solutions. FEM provides the ability to effectively track and analyse the deformation process, which may be difficult to observe in experimental studies. Simulation of the finite element cutting process can enable the analysis of the influence of various technological input parameters, such as cutting clearance, tool edge radius, cutting speed and sheet thickness, etc. on burr height, deformed zone width, stress and strain values in the cutting zone compared to experimental methods. In the available literature, there are many papers devoted to modelling the process of cutting construction materials and light metal alloys. There is a lack of numerical simulations of the process of cutting electrical steels, especially of small thicknesses [4, 14, 23]. This is especially true of the shear-slitting process in which the tools perform a rotary motion.

This paper proposes an approach to modelling the process of cutting electrical steel sheets under real process conditions. The correct determination of the width of individual zones on the cut surface, and thus also the prediction of the occurrence of areas with variable fracture mechanisms using numerical modelling techniques, is currently one of the main difficulties encountered in the literature related to mechanical cutting processes. The new method proposed in the manuscript, based on the analysis of stress triaxiality, enables precise analysis of stress states in the cutting zone and the boundaries of the slipping fracture in the separating fracture, as well as determining the manner of material cracking. The developed models allow for the prediction of stress values and areas of their occurrence depending on the adopted processing parameters.

2. MATERIALS AND METHODS

2.1. Experimental setup

In order to carry out the experiment, a special test stand was designed, shown in Figure 1a. The stand is equipped with a cutting device consisting of rotary knives, a motor, special guides and holders for fixing metal sheets. It allows you to cut sheets in a straight line and cut out rings or circles. A special roller made of polyurethane allows the sheet to be moved horizontally during cutting (Fig. 1b). It is possible to precisely set the value of cutting clearance hc, knife overlap cv and cutting speed v (Fig. 1a, c). The upper knife can be replaced depending on the preferred value of the rake angle α. Before starting the experiments, trial tests of the device were carried out to verify the correct operation. Input, output, disturbing and constant factors were specified. The tests were carried out as follows: prepared electrical steel sheets were mounted in the device and fixed with a special needle. Due to the rotation of the knives and the clamping roll, the cut element was moved along the z-axis, resulting in its separation (Fig. 1b). At the final stage of the process, the attached part remained in place due to the action of the needle, while the cut part fell off. Due to the high complexity and speed of the course of physical phenomena, an advanced vision method (digital image correlation) was used in the cutting process in the form of a specially designed monitoring system, which consisted of a high-speed camera i-SPEED TR, zoom lens, light sources and the GOM Correlate and i-SPEED Suite software. A resolution of 1,280 × 1,024 pixels, and a speed of 2,000 fr/s. were used in images registration. The test stand also includes intermediate rings, LED rings and LED lamps with different diode power. During the experiment, synchronous tracking of points in the recorded sequences of images was carried out. A correlation algorithm was used to create the object model, which may be the first frame of the recorded sequence of test images. The ranges of the variability of the studied factors are summarised in Tab. 1.

sciendo
DOI 10.2478/ama-2024-0038

Tab. 1. The ranges of the variability of the studied factors

Horizontal clearance, h_c	0.02–0.1 mm
Vertical clearance, c_v	0.1 mm
Slitting velocity, v_2	3–24 m/min
Rake angle, α	5°–40°

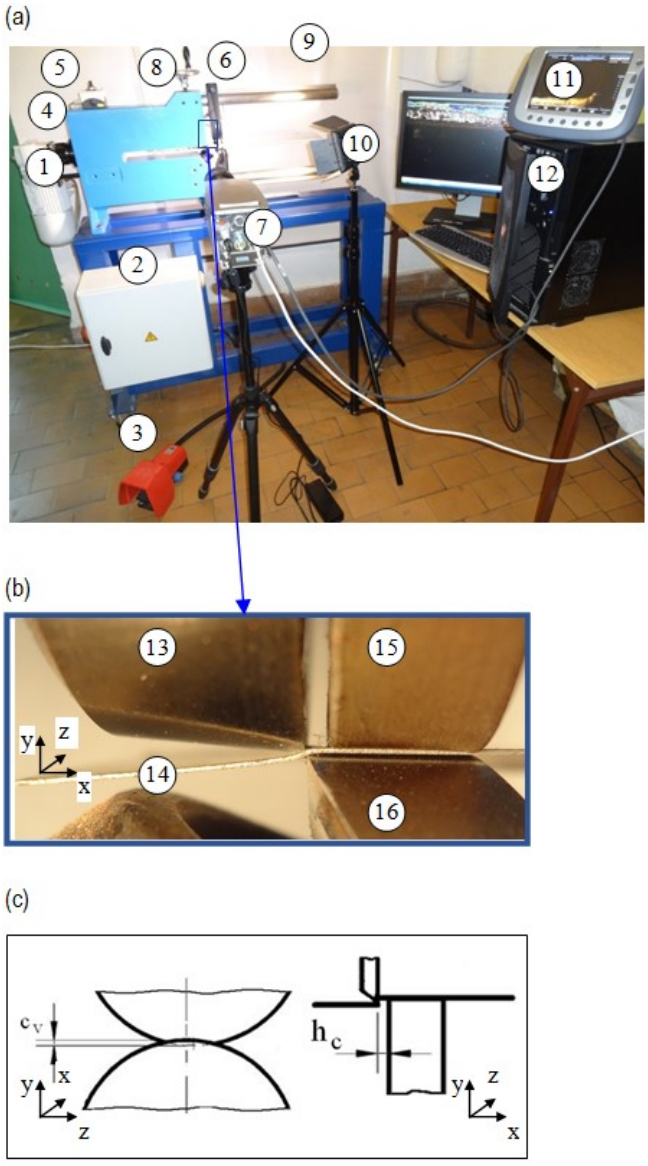

Fig. 1. Experimental test stand: a) 1 – engine, 2 – electrical system, 3 – drive pedal, 4 – threaded socket with a scale for adjusting the cutting clearance, 5 – cutting speed regulator, 6 – sheet stabilizer (needle), 7 – high-speed camera, 8 – knife overlap regulator, 9 – scale for determining the diameter of cut discs for curvilinear outlines, 10 – LED lamp, 11 – auxiliary screen for recording and analysis, 12 – computer workstation for archiving measurement data, b) zoom of contact zone: 13 – upper knife, 14 – sheet, 15 – clamping roll and 16 – lower knife, c) characteristic parameters of the process

2.2. Material characteristics

ET 110-30LS with thickness t = 0.3 mm electrical steel was used in research. Mechanical properties are presented in table 2.

Tab. 2. Mechanical properties of ET 110-30LS steel [34]

Density [kg/dm³]	Yield point [MPa]	Elongation [%]	Hardness [HV_5]
7.8	310 ± 5	14 ± 1.5	170 ± 6

A thickness of t = 0.3 mm was chosen due to this thickness having the greatest applicability for the construction of electrical devices. The mechanical and magnetic properties are presented in Tab. 1 and Fig. 2.

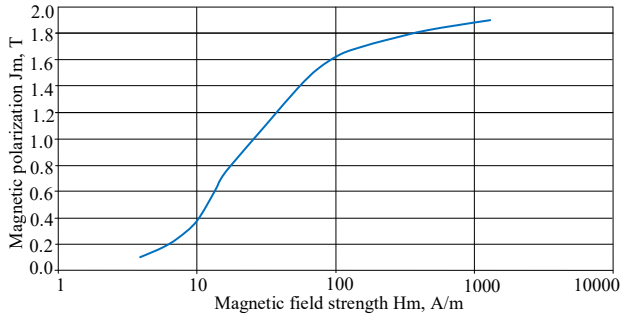

Fig. 2. Magnetisation characteristic J_m=f(H_m) for ET 110-30LS [34].

3. FE MODELLING OF THE SHEAR-SLITTING PROCESS

A mathematical model of the shear-slitting process is incrementally formulated containing the following: a material model, a contact model, an equation of both the motion and deformation, and both the initial and boundary conditions.

3.1. Material modelling

3.1.1. The incremental model of the yield stress

For a typical step time, $t \to \tau = t + \Delta t$, a model $\Delta\sigma_Y$ was defined as [35]:

$$\Delta\sigma_Y = E_T \cdot \Delta\varepsilon_e^{(VP)} + \dot{E}_T \cdot \Delta\dot{\varepsilon}_e^{(VP)}, \quad (1)$$

where $\Delta\varepsilon_e^{(VP)}$ and $\Delta\dot{\varepsilon}_e^{(VP)}$ are the increments of the effective viscoplastic strain and rate, respectively, $E_T \cdot \Delta\varepsilon_e^{(VP)}$ represents the change in the temporary yield stress $\Delta\sigma_Y$ with changing viscoplastic strain, where $E_T = \partial\sigma_Y(\cdot)/\partial\varepsilon_e^{(VP)}$ is the temporary hardening parameter assuming a constant accumulated effective viscoplastic strain rate at time t ($\Delta\dot{\varepsilon}_e^{(VP)} = \text{const}$) and $\dot{E}_T \cdot \Delta\dot{\varepsilon}_e^{(VP)}$ represents the change in the temporary yield stress, σ_Y, with changing viscoplastic strain rate, where $\dot{E}_T = \partial\sigma_Y(\cdot)/\partial\dot{\varepsilon}_e^{(VP)}$ is the temporary hardening parameter assuming a constant accumulated effective viscoplastic strain at time t ($\Delta\varepsilon_e^{(VP)} = \text{const}$).

3.1.2. Elastic/viscoplastic material model

A new mixed hardening model for isotropic materials, which includes the combined effects of elasticity (reversible domain), and viscoplasticity (non-reversible domain) (E/VP), is used. This

DOI 10.2478/ama-2024-0038

model accounts for the mechanic history of the material. The constitutive equation for the incremented components in a total Green–Lagrange strain tensor takes the following form [35, 36]:

$$\Delta\varepsilon_{ij} = \frac{1}{1-\tilde{S}^{**}} \cdot \left(D_{ijkl}^{(E)} \cdot \Delta\sigma_{kl} - \frac{\frac{2}{3}\cdot[\sigma_Y(\cdot)]\cdot\dot{E}_T\cdot\Delta\dot{\varepsilon}_e\cdot\tilde{S}_{ij}}{\tilde{S}_{ij}\cdot C_{ijkl}^{(E)}\cdot\tilde{S}_{kl}+\frac{2}{3}\cdot\sigma_Y^2(\cdot)\cdot\left(\tilde{C}(\cdot)+\frac{2}{3}E_T\right)} \right) \quad (2)$$

Whereas the incremented components for the total second symmetric Pioli–Kirchhoff's stress tensor are as follows [36]:

$$\Delta\sigma_{ij} = C_{ijkl}^{(E)} \cdot \left(\Delta\varepsilon_{kl} - \psi \frac{\tilde{S}_{kl}\cdot\left\{\tilde{S}_{ij}\cdot C_{ijkl}^{(E)}\cdot\Delta\varepsilon_{kl}-\frac{2}{3}\sigma_Y(\cdot)\cdot\dot{E}_T^{(VP)}\cdot\Delta\dot{\varepsilon}_Z^{(VP)}\right\}}{\tilde{S}_{ij}\cdot C_{ijkl}^{(E)}\cdot\tilde{S}_{kl}+\frac{2}{3}\sigma_Y^2(\cdot)\cdot\left(\tilde{C}(\cdot)+\frac{2}{3}E_T\right)} \right) \quad (3)$$

where Δ – increment, ε_{ij} – strain tensor component, σ_{ij}- – stress tensor component, $\tilde{S}^{**} = \tilde{S}_{ij}^{*} \cdot C_{ijmn}^{(E)} \cdot \tilde{S}_{mn}$ is a positive scalar variable, $\tilde{S}_{ij} = S_{ij} - \alpha_{ij}\ (i,j = 1-3)$ is the stress deviator component, $\widetilde{\boldsymbol{D}}_{\sigma}$ and $D_{ijkl}^{(E)}$ is the component for the tensor $\boldsymbol{D}^{(E)} = \boldsymbol{C}^{(E)^{-1}}$in time t, $C_{ijkl}^{(E)}$ are the elastic constitutive tensor components $\boldsymbol{C}^{(E)}$, $\widetilde{C}(\cdot) = \widetilde{C}(\varepsilon_e^{(VP)}, \dot{\varepsilon}_e^{(VP)})$,is the temporary translation hardening parameter in time t, $\sigma_Y(\cdot) = \sigma_Y(\varepsilon_e^{(VP)}, \dot{\varepsilon}_e^{(VP)})$ is the accumulated material yield stress, which depends on the history of the viscoplastic strain and strain rate, and $\varepsilon_e^{(VP)}$and $\dot{\varepsilon}_e^{(VP)}$ are the cumulative effective viscoplastic strain and strain rate, respectively. It is assumed that the relationship of $\sigma_Y(\cdot)$ and $\widetilde{C}(\cdot)$ to $\varepsilon_e^{(VP)}$ and $\dot{\varepsilon}_e^{(VP)}$ can be derived from data obtained during a series of tensile tests at different strain rates using virgin material specimens [37, 38]. The instantaneous value of the yield stress σY was calculated from Johnson-Cook material law [39]:

$$\sigma_Y = [A + B(\bar{\varepsilon}^p)^n][1 + C ln\dot{\varepsilon}^*][1 - (T^*)^m], \quad (4)$$

where: $A, B,$ and n are strain hardening constants, C is the strain rate hardening constant, σ_Y is the equivalent flow stress, $\bar{\varepsilon}^p$ is the equivalent plastic strain, m is the thermal softening constant and $T^*$is the homologous temperature term, where $T^* = \frac{T-T_r}{T_m-T_r}$, T is the temperature of the material, T_r is a reference temperature, and T_m is the melt temperature of the material, $\dot{\varepsilon}^*$ is the normalised strain rate of the material or $\dot{\varepsilon}^* = \frac{\dot{\bar{\varepsilon}}^p}{\dot{\varepsilon}_0}$, where $\dot{\varepsilon}_0 = 1.0s^{-1}$. The model parameters are presented in Tab. 3.

Tab. 3. The Johnson-Cook constitutive model constants for ET 110-30LS steel [34]

$A\ [MPa]$	$B\ [MPa]$	C	n	m
110.4	456	0.049	0.41	0.51

3.2. Simulation model

For the purpose of the work, FEM models were developed in the LS-DYNA solver for the spatial state of stress and the plane (2D) or spatial state of strain (3D) (Figs. 3 and 4). 2D models were used to predict the course of the plastic flow and cracking process in very small cross-sectional areas of the sheet. On the other hand, 3D models, after taking into account the length of the cut line, make it possible to predict deformation and stress states along the cut line and model sheet defects, e.g. bends and corrugations. The models take into account variable rake angle values (α), the value of the radius of the knives, the length of the cutting line and the variable cutting speed. It is also possible to control the setting of overlap c_v.

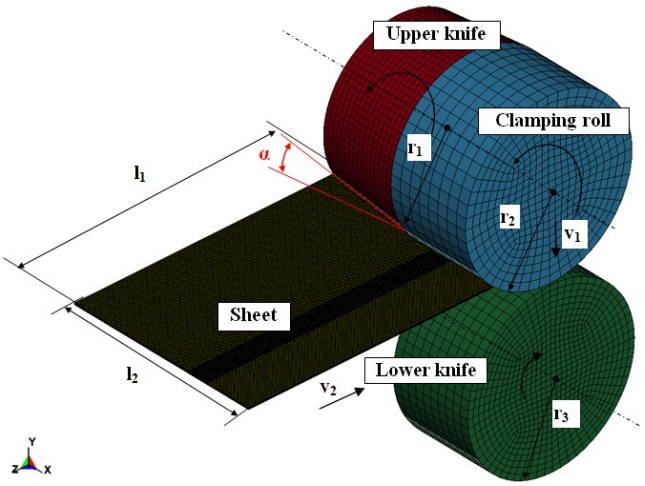

Fig. 3. 3D FE model with boundary conditions

The numerical simulations were carried out for the process control variables in the range of α = 5°–40°, v_2 = 3–32 m/min and h_c = 0.02–0.1 mm. A constant value of tools overlap c_v = 0.1 mm was assumed. The following geometric parameters of the test stand were applied: $r_1 = r_2$ = 15 mm, r_3 = 20 mm, l_1 = 80 mm, l_2 = 40 mm.

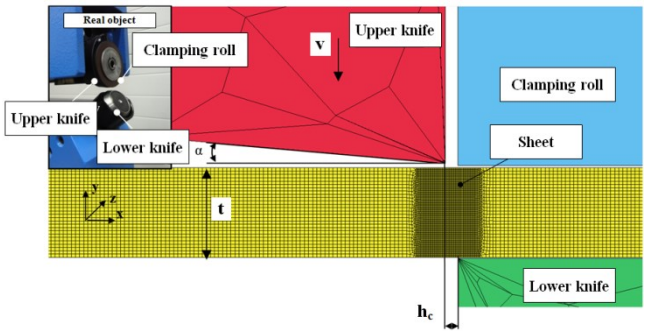

Fig. 4. 2D FE model with boundary conditions

Constant coefficients of static $\mu_s = 0.15$ and dynamic $\mu_d = 0.1$ friction were assumed. A 4-node element of the PLANE 162 type for 2D models and 3D SOLID 164 for 3D models was used to discretise the object.

4. FE MODELLING RESULTS

4.1. Shear-slitting phases and model validation

Since the concentration of maximum deformations and displacements in cutting processes occurs in a small area, advanced vision methods can be used to observe many physical phenomena. Currently, image registration is an important issue in the su-

pervision of manufacturing processes in real time. In this way, it is possible to fully observe the formation of possible product defects. The proposed research methodology uses an advanced vision system for measuring displacements and deformations in the cutting zone, crack propagation moment, trajectory analysis, cracking speed measurement and product quality assessment, depending on the adopted machining parameters at any time during the process.

The proposed method using an advanced vision system was used to analyse deformation states in the cutting zone, crack propagation and crack trajectory. The deformation values and the width of the deformation zone in the material after cutting were also determined. The obtained results were used to validate the simulation results obtained using FEM models.

Fig. 5 shows the plastic flow phase transitioning to the cracking phase of the process. Both in the 2D model and the 3D model, local cracks are visible in the areas of the cutting edges of the knives. Due to the minimal clearance hc used, cracking occurs in the cutting zone and proceeds stably without causing transverse cracking and burr formation, which is consistent with the results obtained experimentally. Particular attention was paid during the comparative analysis to the correct representation of the flow mechanics of the material, the formation of individual zones on the cut surface, among others edge roundness and burrs, the degree of material deformation and the formation of sheared-burnished and fracture zones.

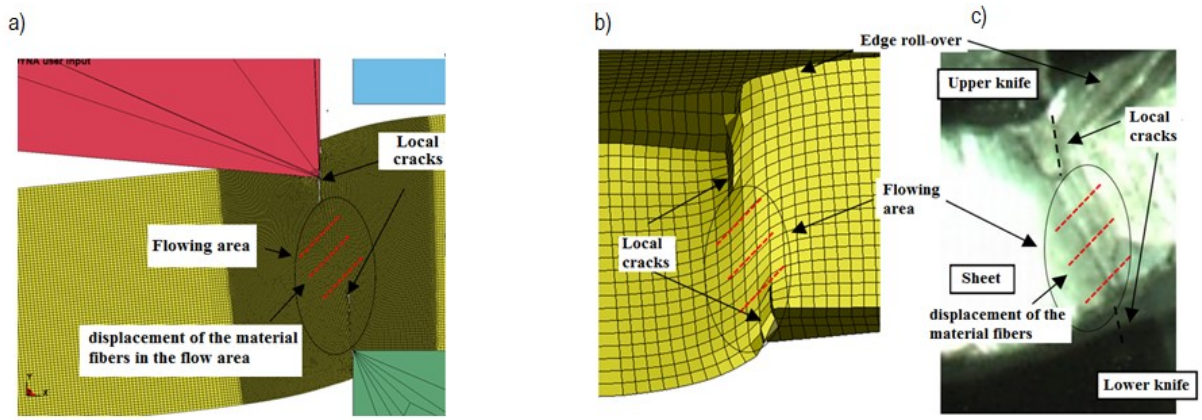

Fig. 5. Numerical representation and visual recording of the transition from plastic flow to cracking: (a) 2D FEM model, (b) 3D FEM, model, (c) camera image (h_c = 0.04 mm, α = 7°, v = 7 m/min).

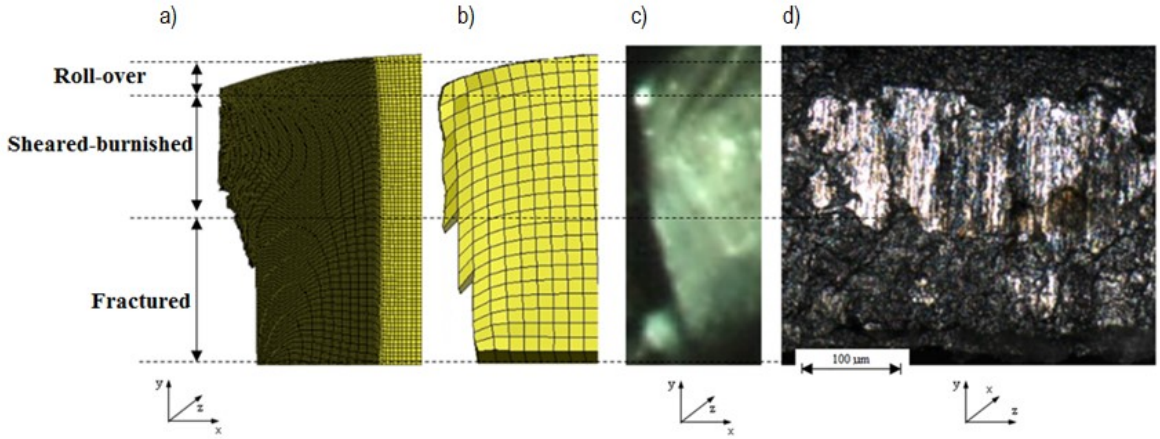

Fig. 6. Analysis of selected features of the cut edge: (a) appearance of the cut edge for the 2D model, (b) appearance of the cut edge for the 3D model, (c) appearance of the cut edge obtained experimentally, (d) image of the surface of the cut edge

Fig. 6 shows the appearance of the cut edge after the cutting process for the configuration of the parameters hc = 0.04 mm, α = 7° and v = 10 m/min. Shaping materials with small thicknesses often causes problems on production lines because (even small deviations from the optimal settings of processing parameters and disturbances cause product defects) they are very sensitive to changes in processing parameters, which causes the formation of burrs and excessive roll-over of the edges. The analyses of the cut edge for the validation of FEM models were made using images recorded with a high-speed camera in the cross-section of the sheet and images of the geometric structure of the cut surface recorded along the cutting line with a LEXT OLS4000 laser confocal microscope from OLYMPUS. The presented example is characterised by a clear transition boundary of the sheared-burnished in the fractured area, which is characterised by the perpendicularity deviation within 40 µm both in simulation models and in the experiment. The rollover zone is acceptable from a technological point of view and is about 30–40 µm. The simulation models correctly reflect the boundaries of the fractures and the size of the roll-over. In the presented case, there is a negligible burr, which was shown in FEM models and confirmed experimentally.

Fig. 7 shows the selected results with clearance hc = 0.08 mm, α = 7° and v = 7 m/min. The effect of the increased clearance on the course of the plastic flow and cracking phases is

DOI 10.2478/ama-2024-0038

particularly visible. In the selected stage of the process phase, the first cracks appear in the contact area of the knife blades with the material. In the 2D model, micro-gaps can be observed near the cutting edges of the knives. In the 3D model, the initial phase of material cracking can be observed. The deformed zone is wider than in the case of reduced clearance cutting and the flow area is non-symmetrical. The fibre arrangement of the material is significantly curved. The asymmetry of the concentration of maximum plastic strains causes uneven and unstable cracking of the material, which does not run in a straight line. Crack propagation proceeds at different speeds. Initially, in the contact zone of the lower knife with the material, the crack propagates faster than in the area under the upper knife, but at a certain stage it stabilises, and due to the movement of the upper knife, cracking accelerates in the area of its contact with the edge of the sheet. The fracture line is far from the knife's cutting edge, resulting in burr formation. Due to the increased bending moment, an increased roll-over of the sheet edges can be observed. The results obtained using FEM models are consistent with the results obtained experimentally, and the characteristic phenomena occurring in the process are correctly predicted. Experimental measurements confirmed the formation of a burr on the lower surface of the sheet edge and a characteristic depression just behind the burr line, which may indicate the area of local micro-cracks.

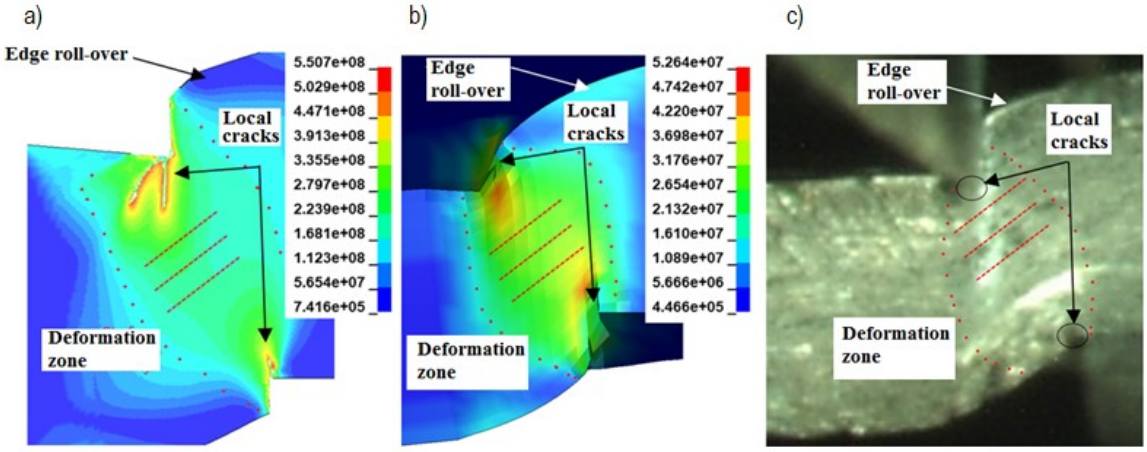

Fig. 7. The course of the plastic flow phase with the beginning of the cracking phase for h_c = 0.08 mm, α = 7°, v = 7 m/min: (a) 2D model, (b) 3D model, (c) camera image

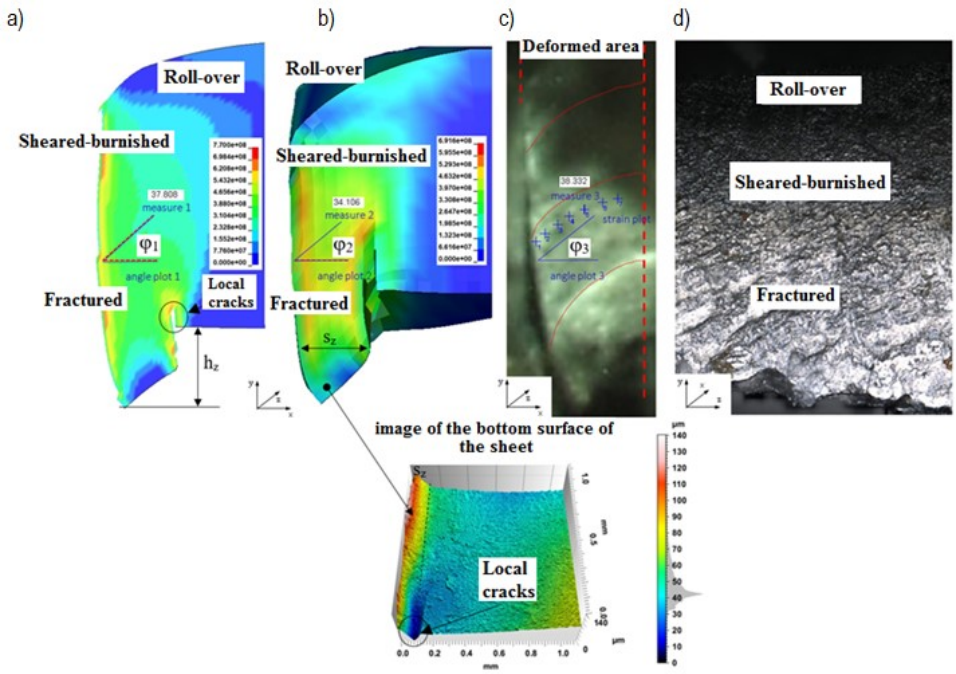

Fig. 8. View of the cut edge after the cutting process for: h_c = 0.08 mm, α = 7°, v = 7 m/min: (a) 2D FEM model, (b) 3D FEM model, (c) camera image, (d) image of the surface of the cut edge, and geometric structure of the lower surface of the sheet in the area of the cut edge

After the cutting process, the following measurements were made: the height of the burr and its width, which are in the range of about h_z = 110–130 µm, s_z = 70–80 µm for both simulation and experiment (Figs. 8a and 8b). It was possible to accurately measure thanks to the option of tracking the displacements of the nodes of the FEM model and the analysis of images of the geometric structure of the bottom surface of the metal sheet registered with a confocal microscope. The flow angle was measured

DOI 10.2478/ama-2024-0038 acta mechanica et automatica, vol.18 no.2 (2024)

using specialised ImageJ and GOM Correlate software. The results of the measurements of the flow angle φ are consistent with the experiment (φ_1 = 37.8°, φ_2 = 34.1°, φ_3 = 38.3°) and do not differ significantly at the assumed significance level (Fig. 8c). The sample is characterised by the lack of a clear transition boundary of the sheared-burnished in the fractured (Fig 8d). In order to predict the area of occurrence of this boundary on the cut edge, a new approach based on the analysis of distributions of the stress triaxiality coefficient was proposed.

4.2. Residual stress analysis

4.2.1. Stress triaxiality distribution

A method, based on stress triaxiality, enables precise analysis of stress states in the cutting area and the boundaries of the zones as well as determining the manner of material cracking. The location of the transition points of individual zones on the cut edge can be determined on the basis of the study of the distribution of the stress triaxiality coefficient η defined as the ratio of hydrostatic stress (hydrostatic pressure) and the equivalent stress (usually calculated using von Mises criterion) [40]. With the use of particular ranges of the triaxiality coefficient developed in the literature, it is possible to predict, using FEM models, characteristic areas of fracture boundaries, even for samples with no clear division boundary. This makes it possible to design tools and select process conditions so as to extend the shearing and plastic flow phase, which causes the formation of a sheared-burnished zone on the cut edge with a minimum share of tensile stresses, causing significant deterioration of magnetic properties.

Figs. 9 and 10 show selected phases of the cutting process with the distribution of the stress triaxiality factor for two values of the cutting clearance hc. In the initial stages, the cutting edges of the tools cause elastic deformation of the material. It is strongly compressed – stresses and elastic strains concentrate near the cutting edges as a result of the elastic bending of the cut material. With a further increase in the load near the cutting edges, plastic deformations occur (Figs. 9a, 10a). Shear areas where the triaxiality coefficient oscillates within the range of η = 0.0 ± 0.16 in the initial phase of the process are close to each other for the two analysed clearance values. Outside the shear area states of uniaxial compression occur in the cross-section of the sheet. In the vicinity of the cutting edges of the tools, there is biaxial compression with significantly negative values of the triaxiality coefficient.

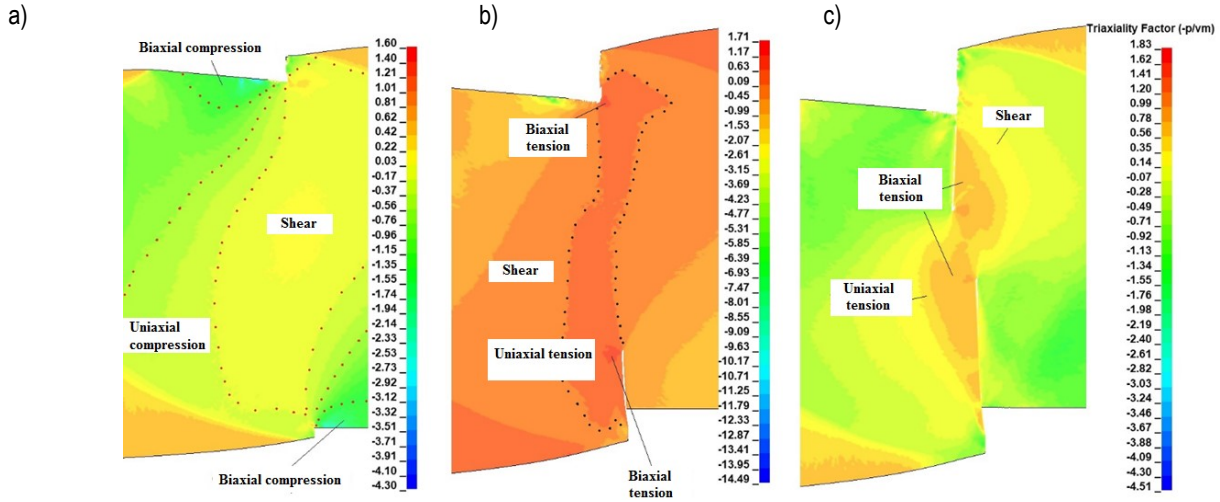

Fig. 9. Triaxiality coefficient values: (a) plastic flow phase, (b) plastic flow phase with a transition to cracking, (c) cracking phase: h_c = 0.02 mm, α = 7º, v = 7 m/min)

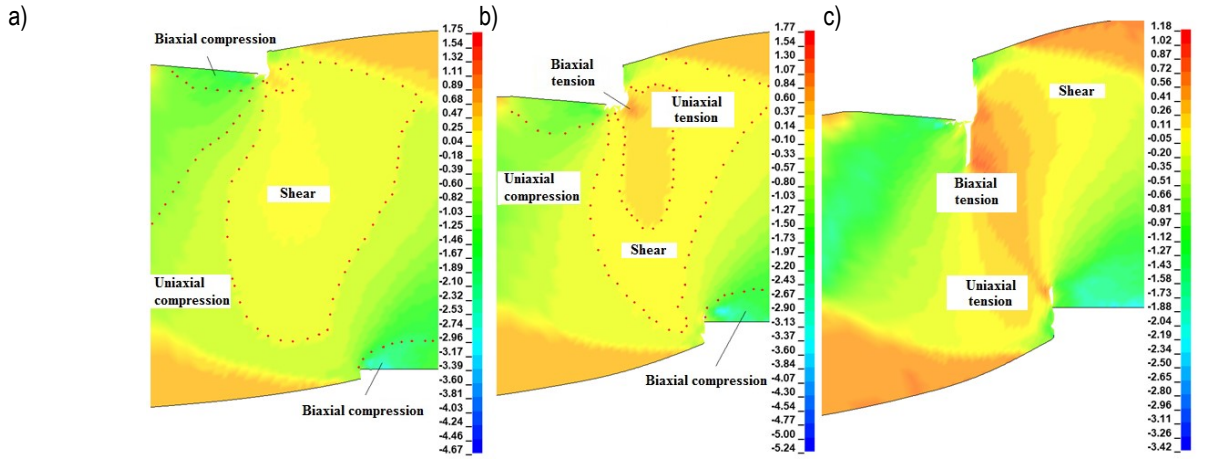

Fig. 10. Triaxiality coefficient values: (a) plastic flow phase, (b) plastic flow phase with a transition to cracking, (c) cracking phase: h_c = 0.08 mm, α = 7º, v = 7 m/min)

DOI 10.2478/ama-2024-0038

In the next stage of the process, the reduced clearance accelerated the cracking process and the formation of a uniaxial stretching zone dominated by the above positive values of the triaxiality coefficient (Fig. 9b). Small areas of biaxial tension are also visible, which can cause micro-cracks in the vicinity of the blades, which was confirmed by experimental studies. For the increased clearance, the shear area occurs at this stage in the lower areas of the sheet thickness (Fig. 10b). Under the upper knife, however, the state of uniaxial tension begins and the transition from the phase of plastic flow to cracking begins. Biaxial tension fields are also visible. In the cracking phase, characteristic distributions of the triaxiality coefficient fields can be observed. For the reduced clearance, the distributions are symmetrical with the separation of areas of biaxial and uniaxial tension of small width along the fracture line (Fig. 9c). For increased clearance, the zone of increased coefficients is wider than for reduced clearance (Fig. 10c). In the fracture line there are states of uniaxial and biaxial tension, and the area of ideal shear is distant from the cut line. When the clearance between the cutting edges of tools is greater than the allowable, as a result of the edge spreading, the bending moment increases, causing excessive bending of the edges of the cut material. As a result, with shearing, there is excessive tension of the material in the gap between the cutting edges, which causes a thick bent burr.

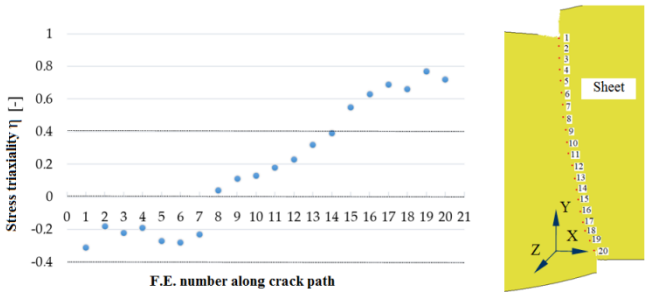

Fig. 11. Triaxiality factor values recorded before removing the finite elements from the mesh in the cracking line: h_c = 0.02 mm, α = 7°, v = 15 m/min

Fig. 11 shows the values of the stress triaxiality factor determined in the finite elements located along the crack path. A sample without a clear fracture separation boundary was selected for the study. Finite elements in the section analysed and lying on the fracture path are marked in Fig. 11. The chart highlights three main areas. The first contains finite elements with negative values of the stress triaxiality coefficient. The second shows the values of the stress triaxiality coefficient in the range from η = 0 to η = 0.4. The third area is the triaxiality of stresses above η = 0.4. The obtained results can be discussed on the basis of analyses of Bao and Wierzbicki's research [41]. The finite elements located in the upper part of the sheet cross-section (elements No. 1–7) were subjected to a shear fracture mechanism and a smooth zone was formed. The features numbered 8–14 were generated by a combination of shear and fracture growth modes. The predicted fracture zone was probably formed by the removal of finite elements from 15 to 20 and was mainly subjected to a mode of fracture formation and growth.

4.2.2. Influence of the process parameters on the residual stresses in the area of the cut edge

Figs. 12–14 show the influence of process parameters on equivalent stresses in the area of the cut edge. The magnetic domain structure is characterised by domains with dimensions similar to the thickness of the sheet and the walls separating them pass through the entire thickness of the sheet and are parallel to the direction of rolling. The plastic deformation of the cut edges causes local displacements of the material, which effectively hinders the movement of the domain walls and domain rotation. As a consequence, this leads to lower permeability, higher coercivity and higher hysteresis losses. In addition, stresses in electrical steel affect the magnetic properties due to the inverse magnetostrictive effect. Fig. 12 shows the influence of the cutting clearance value on the stress values in the cutting zone. The measurement was made in the zone of greatest strengthening in the middle of the cross-section of the sheet. The obtained results confirmed the significant influence of the analysed process parameters on the stress values in the area of the cut surface. In some cases, it can be seen that the maximum stress concentration occurs at a certain distance from the cut surface and not at its edge. In the case of cutting clearances in the h_c = 0.02–0.04 mm range, the concentration of maximum stress values occurs in the area of the cut surface, and their values decrease away from the cut edge. In the case of cutting clearance h_c = 0.06 mm, the maximum stress concentration occurs at a distance of about x_1 = 100 µm from the cut edge. Their values, however, decrease rapidly as they move away from the cut edge. The largest zone of stress concentration occurred for cutting clearances above h_c = 0.08 mm.

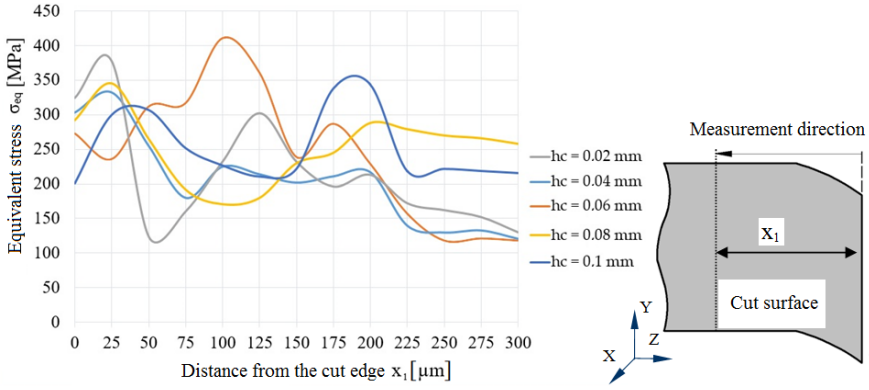

Fig. 12. Influence of cutting clearance h_c on the value of equivalent stresses in the area of the cut edge

The influence of the rake angle of the upper knife cutting edge α on the stress values in the cutting zone is shown in Fig. 13. The value of the angle α has a significant impact on the values of maximum stresses in the cutting zone. The high value of α causes the concentration of maximum stresses directly on the cut edge and their increase compared to α = 7°. For the angle α = 7°, the width of the stress zone is greater than when α = 20° and α = 40°, but their maximum values are smaller.

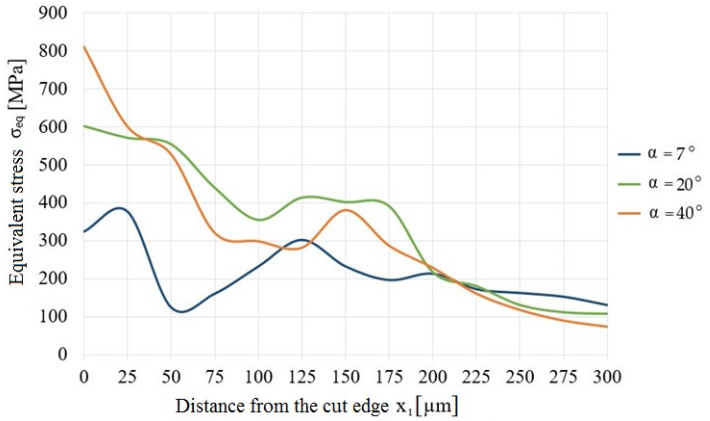

Fig. 13. Influence of rake angle α on the value of equivalent stresses in the area of the cut edge

The influence of cutting speed on the values of equivalent stresses in the cut edge is shown in Fig. 14. In the analysed cases, a significant impact of cutting speed on the values of maximum stresses in the vicinity of the cutting edge can be observed. In the case of cutting with speed *v* = 32 m/min, the maximum stress values cover a larger area of the material than when cutting speeds are lower. For *v* = 3 m/min and *v* = 17 m/min the maximum stress values are lower, which may indicate a reduced width of the plastically hardened zone in the area of the cutting edge.

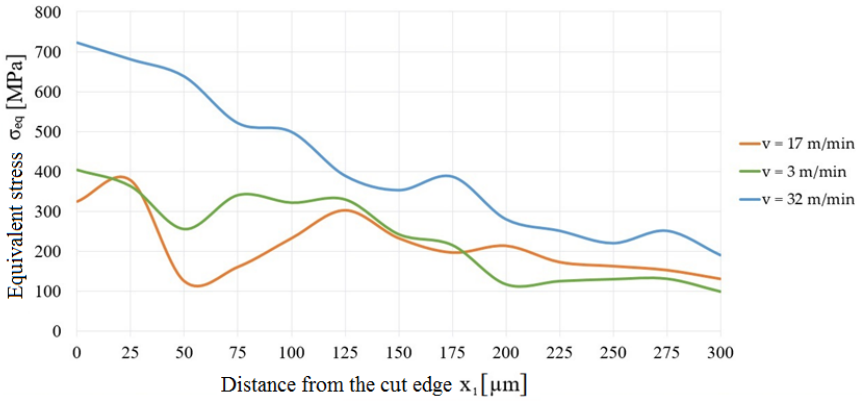

Fig. 14. Influence of cutting speed *v* on the value of equivalent stresses in the area of the cut edge

4.3. Burr formation

The concentration of high stresses and strains in the cutting zone may result in deformation of the cut edge in the form of burrs [42, 43]. The occurrence of burrs on the cut surface is one of the main problems in industrial lines. Parametric analyses of the process were carried out to show which of the machining parameters are crucial and have the greatest impact on burr formation.

The research results indicate that the use of clearances above hc = 0.06 mm causes a significant increase in burr height, regardless of the cutting speed (Fig. 15). This may be due to the fact that the stability of the flow and cracking process decreases, which causes a decrease in the width of the sliding fracture and an increase in the width of the separation fracture and the height of the burr. An increase in clearance above the allowable one causes excessive concentration of the bending moment in the cutting zone.

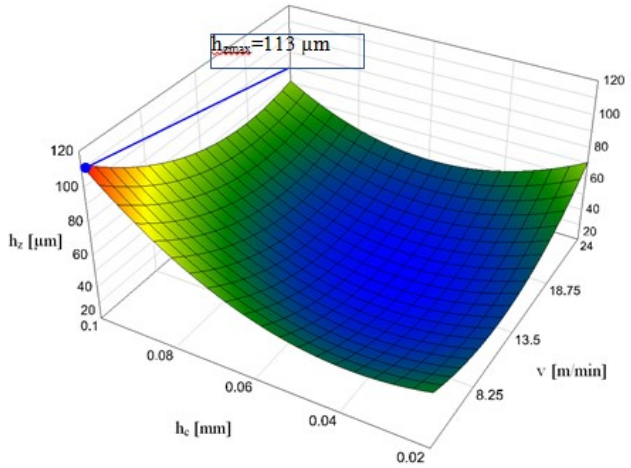

Fig. 15. Influence of cutting speed *v* and clearance h_c on burr height

DOI 10.2478/ama-2024-0038

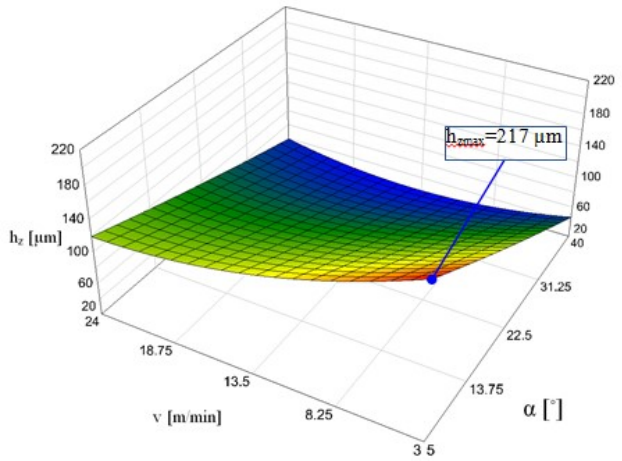

Fig. 16. Influence of cutting speed *v* and rake angle α on burr height

For clearances above h_c = 0.08 mm, the burr height is too large and can be a problem on the production line for each analysed cutting speed. The increase in the burr also contributes to the increase in the rounding and rollover of the edges. Reducing the clearance value to h_c = 0.04 mm makes it possible to increase the cutting speed even to *v* = 24 m/min and obtain an acceptable burr value. For this cutting speed value, the rake angle should be within the range α = 30°–40° (Fig. 16). If the clearance value is less than h_c = 0.04 mm, small angle values α = 5°–18° should be used. In the case of using clearance above h_c = 0.06, it is more advantageous to increase the rake angle. This reduces the bending moment in the cutting area because the contact zone of the knives with the material is smaller and the material cracks earlier.

5. CONCLUSIONS

The process of cutting soft electrical steels is complicated due to the large number of factors affecting the quality of the product. From an industrial point of view, the appropriate quality of the product can be achieved by appropriate control of the process. At the same time, it is important to ensure high process efficiency and reduce the negative impact of process conditions on tool wear and energy consumption. The specificity of electrotechnical materials and their small thickness require very precise settings of machining parameters and process stability. Due to the lack of knowledge on how to control the process, in many cases the amount of waste increases. The paper proposes an approach enabling forecasting the influence of process conditions on product quality. Numerical modelling with the use of finite element analysis was used to analyse the values of stresses, deformations and the quality of the cut edge. As a result, it was determined which conditions can ensure high quality and repeatability of products on production lines and which should be avoided. After the research, the following detailed conclusions can be drawn:

- The obtained research results indicate that there is a limit value of the cutting clearance, after which the stress concentration in the area of the cut edge and the burr increases significantly. This value is for sheet thickness *t* = 0.3 mm, h_c = 0.06 mm.
- It is unfavourable to use a cutting clearance of h_c = 0.08 mm. This causes excessive bending torque and burr formation that can damage the cut edge.
- The correct selection of the cutting clearance is particularly important in the case of high cutting speeds, where with excessive clearance, the stability of the process decreases and the stresses cover the area away from the cut edge by up to 300 µm.
- The value of the tool rake angle should be selected depending on the cutting clearance. With clearances smaller than h_c = 0.04 mm, angle values α = 5°–18° should be used. In the case of using clearance above h_c = 0.06 mm, it is more advantageous to increase the rake angle.
- The results of simulations and experimental tests can be used for the correct selection of machining parameters depending on the adopted criteria.

REFERENCES

1. Jin SY, Pramanik A, Basak AK *et al.* Burr formation and its treatments—a review. International J of Adv Man Tech. 2020; 107: 2189–2210. https://doi.org/10.1007/s00170-020-05203-2
2. Ghadbeigi H, Al-Rubaye A, Robinson FCJ *et al.* Blanking induced damage in thin 3.2% silicon steel sheets. Prod Eng. 2020; 14: 53–64. https://doi.org/10.1007/s11740-019-00931-1
3. Arslan Y, Özdemir A. Punch structure, punch wear and cut profiles of AISI304 stainless steel sheet blanks manufactured using cryogenically treated AISI D3 tool steel punches. Int J of Adv Man Tech. 2016; 87: 587–599. https://doi.org/10.1007/s00170-016-8515-6
4. Falconnet E, Makich H, Chambert J, Monteil G, Picart P. Numerical and experimental analyses of punch wear in the blanking of copper alloy thin sheet. Wear. 2012; 296: 598-606. https://doi.org/10.1016/j.wear.2012.07.031
5. Kurosaki Y, Mogi H, Fujii H. Importance of punching and workability in non-oriented electrical steel sheets. J of Mag and Magn Mat. 2008; 320: 2474–2480. https://doi.org/10.1016/j.jmmm.2008.04.073
6. Lewis N, Anderson P, Hall J, Gao Y. Power loss models in punched non-oriented electrical steel rings. IEEE Trans on Mag. 2016; 52 (5): 1-4. https://doi.org/10.1109/TMAG.2016.2530304
7. Liu Y, Wang Ch, Han H, Shan D, Guo B. Investigation on effect of ultrasonic vibration on micro-blanking process of copper foil. Int J of Adv Man Tech. 2017; 93: 2243-2249. https://doi.org/10.1007/s00170-017-0684-4
8. Boehm L, Hartmann C, Gilch I, Stoecker A, Kawalla R, Wei X, Hirt G, Heller M, Korte-Kerzel S, Leuning N *et al.* Grain size influence on the magnetic property deterioration of blanked non-oriented electrical steels. Materials. 2021; 14: 7055. https://doi.org/10.3390/ma14227055
9. Wilczyński W. Wpływ technologii na właściwości magnetyczne rdzeni maszyn elektrycznych. IEI Warszawa 2003 (in Polish).
10. Miyagi D, Miki K, Nakano M, Takahashi N. Influence of compressive stress on magnetic properties of laminated electrical steel sheets. IEEE Trans of Mag. 2010; 46: 318-321. https://doi.org/10.1109/TMAG.2009.2033550.
11. Naumoski H, Riedmüller B, Minkow A. Herr U. Investigation of the influence of different cutting procedures on the global and local magnetic properties of non-oriented electrical steel. J of Mag and Magn Mat. 2015; 392: 126–133.https://doi.org/10.1016/j.jmmm.2015.05.031
12. Xiong X, Hu S, Hu K, Zeng S. Texture and magnetic property evolution of non-oriented Fe-Si steel due to mechanical cutting, Jof Magn and Magn Mat. 2016; 401: 982-990. https://doi.org/10.1016/j.jmmm.2015.10.023
13. Leuning N, Steentjes S, Schulte M, Bleck W, Hameyer K. Effect of elastic and plastic tensile mechanical loading on the magnetic properties of NGO electrical steel. J of Magn and Magn Mat. 2016; 417: 42-48. https://doi.org/10.1016/j.jmmm.2016.05.049
14. Wang X, Wang Z, Cui R, Li Sh. Influence of blanking process on the magnetic properties of non-oriented electrical steel lamination. J of Shan Jiao Tong Univ. 2019; 53(9): 1115-1121. https://doi.org/10.1109/TMAG.2018.2799839

15. Wang N, Golovashchenko S.F. Mechanism of fracture of aluminum blanks subjected to stretching along the sheared edge. J of Mat Proc Tech. 2016; 233: 142–160. https://doi.org/10.1016/j.jmatprotec.2016.02.022
16. Falconnet E, Chambert J, Makich H, Monteil G, Winter S, Nestler M, Galiev E, Hartmann F, Psyk V, Kräusel V, Dix M. Adiabatic blanking: Influence of clearance, impact energy, and velocity on the blanked surface. J of Man and Mat Proc. 2021; 5: 35.
17. Molitor D.A, Kubik C, Hetfleisch R.H, Groche P. Workpiece image-based tool wear classification in blanking processes using deep convolutional neural networks. Prod Eng. 2022; 1-12. https://doi.org/10.1007/s11740-022-01113-2
18. Mucha J, Jaworski J. The quality issue of the parts blanked from thin silicon sheets. JMEPEG. 2017; 26: 1865–1877. https://doi.org/10.1007/s11665-017-2589-7
19. Toda H, Zaizen Y, Namikawa M, Shiga N, Oda Y, Morimoto S. Iron loss deterioration by shearing process in non-oriented electrical steel with different thicknesses and its influence on estimation of motor iron loss. IEEJ J of Ind Appl. 2014; 3 (1): 55-61. https://doi.org/10.1541/ieejjia.3.55
20. Omura T, Zaizen Y, Fukumura M, Senda K, Toda H. Effect of hardness and thickness of nonoriented electrical steel sheets on iron loss deterioration by shearing process. IEEE Trans on Magn. 2015; 51 (11). https://doi.org/10.1109/TMAG.2015.2443176
21. Schoppa A, Schneider J, Roth J.O. Influence of the cutting process on the magnetic properties of non-oriented electrical steels. J of Magn and Magn Mat. 2000; 215-216: 100-102. https://doi.org/10.1016/S0304-8853(00)00077-9
22. Rygal R, Moses A. J, Derebasi N, Schneider J, Schoppa A. Influence of cutting stress on magnetic field and flux density distribution in non-oriented electrical steels. J of Magn and Mag Mat. 2000; 215–216: 687–689. https://doi.org/10.1016/S0304-8853(00)00259-6
23. Subramonian S, Altan T, Campbell C, Ciocirlan B. Determination of forces in high speed blanking using FEM and experiments. J of Mat Proc Tech. 2013; 213: 2184-2190. https://doi.org/10.1016/j.jmatprotec.2013.06.014
24. Wang Z, Li S, Cui R, Wang X, Wang B. Influence of grain size and blanking clearance on magnetic properties deterioration of non-oriented electrical steel. IEEE Trans on Magn. 2018; 54 (5): 1–7. https://doi.org/10.1109/TMAG.2018.2799839
25. Winter K, Liao Z, Ramanathan R, Axinte D, Vakil G, Gerada C. How non-conventional machining affects the surface integrity and magnetic properties of non-oriented electrical steel. Mat and Des. 210. 2021. https://doi.org/10.1016/j.matdes.2021.110051
26. Smudde CM, D'Elia CR, San Marchi CW, Hill MR, Gibeling JC. Effects of residual stress on orientation dependent fatigue crack growth rates in additively manufactured stainless steel. Int J of Fat. 2023; 169: 107489. https://doi.org/10.1016/j.ijfatigue.2022.107489
27. Khatri N, Barkachary BM, Muneeswaran B, Al-Sayegh R, Luo X, Goel S. Surface defects incorporated diamond machining of silicon. Int J of Extr Man. 2020; 2(4): 045102. https://doi.org/10.1088/2631-7990/abab4a
28. Zhao Y, Wang S, Yu W, Long P, Zhang J, Tian W, Gao F, Jin Z, Zheng H, Wang C et al. Simulation and Experimental Study of Laser Processing NdFeB Microarray Structure. Micromachines 2023; 14: 808. https://doi.org/10.3390/mi14040808
29. Leuning N, Jaeger N, Schauerte M, Stöcker B, Kawalla A et al. Material design for low loss non-oriented electrical steel for energy efficient drives. Materials 2021; 14: 6588. https://doi.org/10.3390/ma14216588
30. Molitor DA, Kubik C, Hetfleisch RH, Groche P. Workpiece image-based tool wear classification in blanking processes using deep convolutional neural networks. Prod Eng. 2022; 1-12. https://doi.org/10.1007/s11740-022-01113-2
31. Kamarul Adnan AA, Azinee SN, Norsilawati N, Izzul KAM. Analysis of the influence of the blanking clearance size to the burr development on the sheet of mild steel, brass and aluminium in blanking process. J of Ach in Mat and ManEng 2022;111(1):26-32. https://doi.org/10.5604/01.3001.0015.9093.
32. Dzidowski ES. Mechanizm pękania poślizgowego w aspekcie dekohezji sterowanej metali. Wydawnictwo Politechniki Wrocławskiej. Wrocław 1990 (in Polish).
33. Gutknecht F, Steinbach F, Hammer T, Clausmeyer T, Volk W, Tekkaya AE. Analysis of shear cutting dual phase steel by application of an advanced damage model, 21st European Conference on Fracture ECF21. 20-24 June 201. Catania Italy. Procedia Structural Integrity. 2016; 2:1700-1707. https://doi.org/10.1016/j.prostr.2016.06.215
34. Kułakowski M. Badania wpływu parametrów i warunków procesu cięcia mechanicznego na lokalne zmiany właściwości laserowanych blach elektrotechnicznych. Rozprawa doktorska. Politechnika Koszalińska. Koszalin 2023 (in Polish).
35. Kukielka L, Kulakowska A, Patyk R. Numerical modeling and simulation of the movable contact tool-worpiece and application in technological processes. Jof Syst. Cyb and Inf. 2010; 8(3): 36-41.
36. Kukielka L. Nonlinear modeling for elasto/visco – plastic contact problem in technological processes, International Scientific IFNA – ANS Journal, Problems of non – linear Analysis in Engineering Systems 2004;2:39-53.
37. Kałduński P, Kukiełka L. The numerical analysis of the influence of the blankholder force and the friction coefficient on the value of the drawing force. PAMM 2007; 7 (1): 4010045-4010046. https://doi.org/10.1002/pamm.200701059
38. Kałduński P, Kukiełka L. The sensitivity analysis of the drawpiece response on the finite element shape parameter. PAMM. 2008; 8 (1): 10725-10726. https://doi.org/10.1002/pamm.200810725
39. Johnson GR, Cook WH. Fracture characteristics of three metals subjected to various strains, strain rates, temperatures and pressures. Eng Frac Mech. 1985; 21 (1): 31-48. https://doi.org/10.1016/0013-7944(85)90052-9
40. Rickhey F, Hong S. Stress triaxiality in anisotropic metal sheets—definition and experimental acquisition for numerical damage prediction. Materials. 2022; 15(11):3738. https://doi.org/10.3390/ma15113738
41. Bao Y, Wierzbicki T. On fracture locus in the equivalent strain and stress triaxiality space. Int J of Mech Sci. 2004; 46: 81-98. https://doi.org/10.1016/j.ijmecsci.2004.02.006
42. Kuo SK, Lee WC, Lin SY, Lu CY. The influence of cutting edge deformations on magnetic performance degradation of electrical steel. 2014 17th International Conference on Electrical Machines and Systems (ICEMS) 2014; 3041-3046. https://doi.org/10.1109/ICEMS.2014.7014017
43. Cao H, Hao L, Yi J, Zhang X, Luo Z, Chen Sh et al. The influence of punching process on residual stress and magnetic domain structure of non-oriented silicon steel. J of Mag and Magnetic Materials. 2016; 406: 42–47. https://doi.org/10.1016/j.jmmm.2015.12.098

Łukasz Bohdal: https://orcid.org/0000-0002-8085-9530
Agnieszka Kułakowska: https://orcid.org/0000-0001-5506-5440